

Black Coloured Glazes with Tetragonal CuCr_2O_4 Ceramic Pigment as Selective Solar Absorbers for Integral Ceramic Solar Collectors

G. Monrós^{1,*}, C. Delgado¹, G. Monrós-Andreu², J. Badenes¹ and M. Llusar¹

¹Department of Inorganic and Organic Chemistry, University Jaume I, Castelló, Castelló, Spain

²Department of Mechanic Engineering and Construction University Jaume I, Castelló, Castelló, Spain

Abstract: An efficient and low-cost Selective Solar Absorber for integral ceramic solar collectors, based in glazes pigmented with t- CuCr_2O_4 and Sb modified t- CuCr_2O_4 pigments, are characterised and evaluated. The basic kinds of industrial glazes (soda lime glass, double firing glaze 1050 °C and both single firing glazes of 1080 °C and porcelain glaze of 1190 °C) have been checked and characterised by CIEL*a*b* colour, UV-Vis-NIR diffuse reflectance spectra, bandgap measurements, SEM-EDS analysis and solar absorbance spectra. The characteristics of the black powders ($L^*a^*b^*$ and diffuse reflectance spectra with a deviation from the carbon black $\Delta E^*=20.3$ and 22.3 respectively) are improved in 0.5 wt% addition of pigments in soda lime glass ($\Delta E^*=6.1$ and 9.9 respectively) and in 5 wt% glazed in porcelain glaze 1190 °C ($\Delta E^*=12.0$ and 18.4 respectively) which can be considered as low-cost selective solar absorbers (SSA) for integral solar absorber collectors.

Keywords: Ceramic pigment, Alkaline earth, Perovskite, Chromium.

1. INTRODUCTION

The ideal selective solar absorber (SSA) material should be low-cost, easy to form, strong (in terms of pressure and handling), stable at 200 °C at least, stable to long exposure to ultraviolet radiation, nonporous, light weight and non-corrosive. Therefore, an optimised and low-cost selective solar absorber (SSA) is required to efficiently use the thermal energy derived from solar radiation using FPSC (flat-plate solar collector) [1].

Recently, an integrally build by ceramic materials ("All-ceramic solar collector"), has been reported using low porosity ceramic plates with a network of ducts inside through which the liquid collector circulates, the dried and shaped plate is coated with an slurry of the "V-Ti black" ceramic pigment (the authors probably refer to the grey of V-TiO₂ [2] or the grey of V,Sb-TiO₂ CPMA 11-21-8 [3]) and the assembly are single fired at 1210 °C [4]. The fluid passages are integrated with the absorber plate, which ensure good thermal conductance between them. The thermal conductivity of ceramics is lower than metals. However, an enrichment of the ceramics with alumina and the entire collector area in contact with the thermal transfer fluid, allow to a good efficiency of heat transfer [5]. Figure 1 illustrates the concept of Integral Ceramic Solar Collector with a ceramic body as carrier of the heat exchange tubes and the proposed selective solar absorber (SSA): a black glaze pigmented with tetragonal CuCr_2O_4 .

Absorber coating is the most important part of the collector. An ideal selective solar absorber maximises solar absorptance in the solar spectrum range (300–2500 nm) and shows low thermal emittance in the infrared wavelength range ($\lambda > 2500$ nm). The spectral transition between the region of high absorbance and low emittance (cut-off wavelength) should be as sharper possible. For energy applications, the cut-off wavelength should be around 2000 nm, which is the limit of the solar spectrum [6].

Therefore, in order to achieve SSA pigments, the following factors should be considered:

a) Presence of highly absorbing species in the Vis-NIR range (400-2500 nm), that is, an ideal black body without reflectance in this range or a 100% of absorbance of Vis-NIR Solar Radiation α :

$$\alpha = \frac{\int_{400}^{2500} (1-r(\lambda))i(\lambda)d\lambda}{\int_{350}^{2500} i(\lambda)d\lambda} \quad (1)$$

where $r(\lambda)$ is the spectral reflectance (Wm^{-2}) measured by UV-Vis-NIR spectroscopy and $i(\lambda)$ is the standard solar irradiation ($\text{Wm}^{-2} \text{nm}^{-1}$) according to the American Society for Testing and Materials (ASTM) Standard G173-03.

Likewise, it is interesting that it presents high reflectance in the UV range (100-400 nm) for block UV radiation and protect organic binders.

b) High thermal emittance ε that measures the ability to release heat that it has absorbed for a material, and therefore, its temperature is moderated [7].

$$\varepsilon = \frac{\int_{2500}^{20000} (1-r(\lambda))E(\lambda,T)d\lambda}{\int_{2500}^{20000} E(\lambda,T)d\lambda} \quad (2)$$

*Address correspondence to this author at the Department of Inorganic and Organic Chemistry, University Jaume I, Castelló, Castelló, Spain; Tel: 34-(0)964 728250; Fax: 34-(0)964 728214; E-mail: monros@uji.es

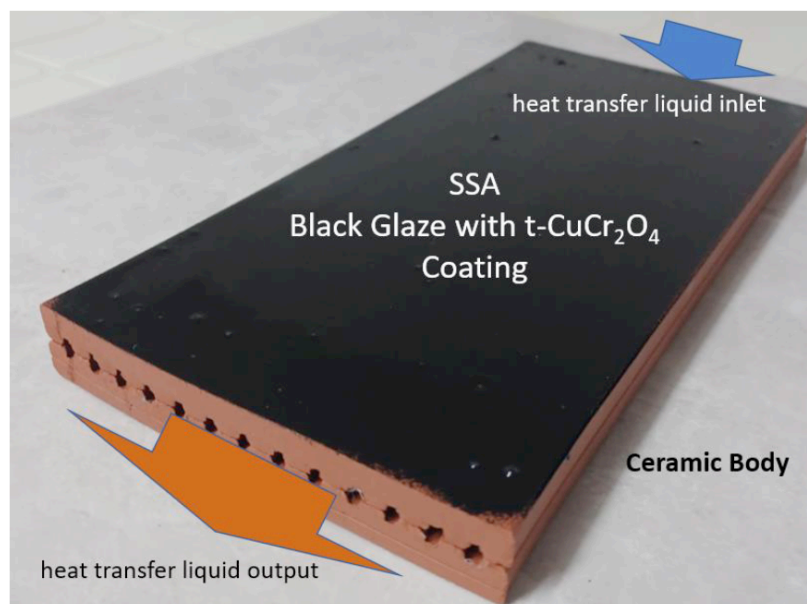


Figure 1: Integral Ceramic Solar Collector concept.

where $r(\lambda)$ is the spectral reflectance (Wm^{-2}) measured by UV-Vis-NIR spectroscopy and $E(\lambda, T)$ is the blackbody radiation spectrum at the considered temperature ($\text{Wm}^{-2} \text{nm}^{-1}$) [8]. The emittance index of solids is high (e.g. ceramics 0.9, asphalt 0.88) except in the case of conductive metals (e.g. Ag 0.02, Al 0.03, Cu 0.04).

Cubic CuCr_2O_4 is fully ordered normal spinel (space group $Fd\text{-}3m$) at temperatures above 853K: Cr^{3+} ($3d^3$) occupies the octahedral sites because of the strong crystal field stabilization of the half occupied nondegenerate t_{2g} states and empty e_g states, while Cu^{2+} ($3d^9$) occupies the $\frac{1}{2}$ of tetrahedral sites in the FCC oxygen lattice. The tetrahedral crystal field around Cu^{2+} ($3d^9$) in the cubic phase results in fully occupied low-energy e levels and triply degenerate t_2 levels, rendering this structure potentially unstable. The Jahn Teller distortion from cubic to tetragonal symmetry ($I41/amd$ space group) lifts the orbital degeneracy in CuCr_2O_4 at 853 K. CuO_4 tetrahedra are compressed toward a square planar configuration, thus lifting orbital degeneracy [9].

The tetragonal polymorph $t\text{-CuCr}_2\text{O}_4$, stable at room temperature, is a p-type semiconductor applied in various catalyst fields because of peculiar physical and chemical properties [10], and it has attracted attention due to its promising application for solar absorber coating [11]. A variety of synthetic methods have been used such as hydrothermal, coprecipitation, sol-gel, etc. in the preparation of CuCr_2O_4 catalysts [12]. In most of these methods, the drawbacks tend to be the high reaction temperature, the long reaction time and the complex reaction strategies as well as the use of very expensive precursors with a more diverse and intense

hazard classification (synthetic and purified inorganic salts, synthetic organic salts or metal alkoxides).

For the synthesis of ceramic pigments, the use of oxide or carbonate precursors, usually obtained directly from nature, and the precursors for the synthesis of the above-mentioned salts, as well as the use of the simple ceramic method by solid state reaction (grinding and calcining the mixture), allow to obtain sintered materials with high pigmenting performance. The evaluation of LCA (Life Cycle Analysis) is usually favourable to this methodology compared to non-conventional methods, only of interest when the solid-state reaction requires very higher temperatures, or the characteristics of the material obtained require its use (case of heteromorphic pigments such as iron encapsulated in silica, or colloidal pigments, such as the classic Cassius purple) [13, 14].

It is very important consider the concept of "pigment"; it is not only a coloured substance, but rather a colored substance that remains stable and imparts colour to the matrices to be pigmented when added in reasonable concentrations (between 0.5 and 5 wt.%) [13, 14]. CPMA (Color Pigments Manufacturers Association of U.S.A) [3], classifies the pigments in three categories: (a) Category A deals with pigments suspended in glass matrixes which require the highest degree of heat stability and chemical resistance to withstand the attack of molten glass. They are predominantly (but not exclusively) used for coloring ceramic glazes, ceramic bodies, porcelain enamels, glass enamels, roofing granules, and other coatings of high temperature performance requirements, (b) Category B deals with pigments suspended in plastics and other polymers which require only moderate heat

stability, and (c) Category C deals with pigments suspended in liquid vehicles which require little, or no heat stability.

But within Category A (ceramic pigments) it is very important to distinguish between the main families of ceramic frits in the conventional glazed tile industry (the conventional soda-lime glass is also considered) [13, 14]:

I. Milled glass. The conventional soda-lime glass is composed basically of silica, sodium oxide and lime which softens at a moderate temperature (around 550 °C) with short maturation times (5 min) at the maximum temperature (800 °C) in a short firing cycle of 67 min. Table 1 shows the approximate oxide composition of the milled glass used in this study.

II. Double firing lead-free. The high volatility of lead above 1150 °C (usually used up to 1980) at temperatures above 1100 °C make its use of little interest due to the losses during firing and the instability of the stoichiometry of the glaze. Likewise, the high toxicity of lead (Threshold Limit Value–Time-Weighted Average (TLV–TWA) airborne levels of chemical exposure on a weekly average of 40 hours, 0.15 mg/m³ at 20°C and 101.3 kPa and biological limit of 70 mg/dL in blood) forbids its use [15].

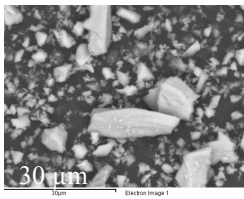
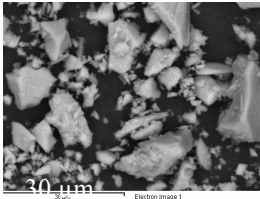
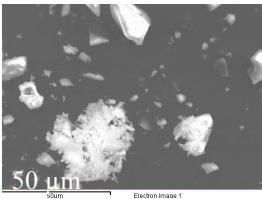
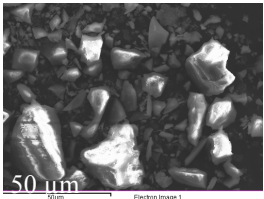
In the formulations of transparent enamels for rapid double-firing cycles without lead, its flux is replaced by potash or boron oxide and alkaline earth metals (CaO) and/or ZnO. With these formulations, the glaze softens at a moderate temperature with low viscosity in the melt using short maturation times at the maximum

temperature (between 3-5 min). Table 1 shows the approximate oxide composition of the transparent frit for lead-free double firing used in this study. The firing cycle for this frit shows a maximum temperature of 1050 °C (5 min) with a total duration of 67 minutes

III. Single firing frit for porous stoneware (monoporosa). When introducing single firing with porous pastes with calcium carbonate contents greater than 7 wt%, it is necessary to formulate glazes that seal at a temperature higher than the thermal treatment of the carbonates to avoid deterioration of the enamel layer and formation of bubbles. which also requires it to mature in a short temperature range. These requirements are achieved by the addition of alkaline earth metals (CaO and MgO) and ZnO, maintaining a balanced charge of fluxes based on alkali metals and boron oxide. Table 1 shows the oxide composition of the single firing transparent frit for monoporosa used in the present study. The firing cycle for this frit shows a maximum temperature of a maximum temperature of 1080 °C (5 min) with a duration of 67 minutes.

IV. Single-firing porcelain frit. The porcelain stoneware pastes based on a triaxial mixture of clays, feldspars and quartz produce very low porosity (less than 0.2 wt%), which allows their use in outdoor environments given their high resistance to frost. The vitreous enamels that waterproof these pastes must be formulated so that they mature at the firing temperature of the paste (between 1180 and 1200 °C) with CaO-ZnO-Al₂O₃ base compositions together with SiO₂. Table 1 shows the approximate oxide composition of the transparent frit for porcelain stoneware used in this

Table 1: SEM Micrograph and Estimated Compositions by EDS of Employed frits

	Glass 800 °C	Double Firing 1050 °C	Single Firing 1080 °C	Single Firing 1190 °C
Oxide				
SiO ₂	74	59	65	67
Na ₂ O	13	4	2	-
K ₂ O	0.5	5	4	3
CaO	11	15	11	12.5
MgO	-	-	2	1.5
ZnO	-	9	7.5	6
Al ₂ O ₃	1.5	8	8.5	10
PbO	-	-	-	-

study. The firing cycle for this frit shows a maximum temperature of 1190 °C (5 min) and a duration of 57 minutes.

For an integral ceramic flat-plate solar collector, the drawbacks of the direct coating with the selective solar absorber powder tend to be the high reaction temperature, the low adherence of the powder, the uncontrolled final surface morphology and the instability of the pigment at the firing temperatures. Glazing the ceramic support of the integral ceramic collector with a glaze, containing only between 2-5 wt% of the pigment, avoids the above-mentioned problems: minimise the cost, given the low pigment addition, waterproofs the active surface of collector, and likewise, the morphology and reflectance of the final surface are controlled and reproducible.

To our knowledge, the characterization of (t- CuCr_2O_4)-glaze composites (or coloured glazes with tetragonal cuprochromite) as selective solar absorber for integral ceramic solar collectors are not documented (Figure 1). In this study tetragonal CuCr_2O_4 has been prepared by solid state reaction method from oxides and both powder and glazed ceramic samples have been characterized as black material for low-cost selective solar absorber (SSA). On the other hand, the addition of Sb_2O_3 (formal stoichiometry $\text{Cu}(\text{Cr}_{1.9}\text{Sb}_{0.1}\text{O}_4)$) has been studied to control the cut-off wavelength and enhance the IR emittance of the SSA by composite-effect [16].

2. EXPERIMENTAL

Solid-state or ceramic procedure has been used for the synthesis of CuCr_2O_3 (sample 1B) and $\text{Cu}(\text{Cr}_{1.9}\text{Sb}_{0.1}\text{O}_4)$ (sample 1BSb) compositions from the respective oxides as precursors, with a particle size between 0.3–5 μm : tenorite CuO , eskolaite Cr_2O_3 and antimony (III) oxide Sb_2O_3 supplied by QUIMIALMEL SA (99.5 wt% quality). The precursors were mechanically homogenized in an electric grinder (20,000 rpm) for 5 min. The mixture was then fired at 1000 °C for 3 hours.

The samples were characterised by the following techniques:

X-ray Diffraction (XRD) was performed on a Siemens D5000 diffractometer using Cu K_α radiation (10–70° 2θ range, scan rate 0.02° 2θ , 4 s per step and 40 kV and 20 mA conditions). From the ($^\circ 2\theta$) positions of the diffraction peaks, the volume of the tetragonal cell ($a^2 \times c$) was calculated using Equation (3):

$$\frac{1}{d^2} = \frac{h^2+k^2}{a^2} + \frac{l^2}{c^2} \quad (3)$$

where d is the interplanar distance of the respective (hkl) lattice plane, obtained from $^\circ 2\theta$ using Bragg's law

and $a=b$ and c are the tetragonal cell edges. For glazed samples grazing or low angle of incidence X-ray diffraction was carried out on a Siemens D5000 diffractometer using similar conditions that for conventional diffractometry. The study of thin layers by conventional diffractometry is limited, with low angle incident X-ray the penetration of the X-rays into the sample is much greater than the thickness of the layer for detect the underlying crystals

The $L^*a^*b^*$ and C^*h^* colour parameters of the glazed samples were measured following the CIE- $L^*a^*b^*$ (Commission Internationale de l'Éclairage) [17] colorimetric method using an X-Rite SP60 spectrometer with standard lighting D65 and a 10° observer, as described above. In this method L^* measures the lightness (100=white, 0=black) and a^* and b^* the chroma ($-a^*$ =green, $+a^*$ =red, $-b^*$ =blue, $+b^*$ =yellow). The CIEL $^*C^*h$ colour space correlates well with color perception by the human eye; C^* represents chroma [18] and h^* is the hue angle that can be estimated from parameters a^* and b^* using Equations 4 and 5, respectively.

$$C^* = (a^{*2} + b^{*2})^{1/2} \quad (4)$$

$$h^* = \arctan(b^*/a^*) \quad (5)$$

The tolerance ΔE^* (based on the $L^*a^*b^*$ parameters), is evaluated using eq. 6:

$$\Delta E^* = \sqrt{\Delta L^{*2} + \Delta a^{*2} + \Delta b^{*2}} \quad (6)$$

UV-Vis-NIR spectra of both the fired powder and glazed samples were collected with a Jasco V670 spectrometer using the diffuse reflectance technique, which provides data in absorbance or reflectance units (R (%)). The bandgaps of the samples were estimated using the Tauc method [17]. The total solar reflectance was evaluated from UV-Vis-NIR spectra using the diffuse reflectance technique, and both absorbance and emittance are estimated as above described (eq. 1,2).

The colouring capacity of the corresponding pigment was studied in four matrices above described: (a) 0.5w% glazed in milled glass (800 °C), (b) 5w% glazed double firing frit 1050 °C of maturation point), (c) 5wt.% glazed in single firing frit 1080°C, (d) 5wt.% glazed in porcelain single firing frit 1190 °C. The glazed samples were prepared using substrates of white stoneware tiles coated with glaze prepared by manual mixing of frit, pigment and water in a weight ratio of 97:5:40 in an agata mortar, with a thickness (~1500 μm) using the Doctor Blade technique. Molten glazes attack pigment particles by dissolving or reacting with them, resulting in some degradation or alteration of colour. The aggressiveness of the glaze increases with

the maturation temperature and chemical composition (increases in sequence I-IV). A good ceramic pigment should maintain its pigmentation capacity in aggressive glazes.

3. RESULTS AND DISCUSSION

3.1. Characterization of Glazes and Modifier

Table 1 shows the SEM micrograph and estimated compositions by EDS of employed frits that have been above described. All frits were milled to a particle size between 1-15 μm as shows the SEM images. The presence of alkalis decreases and the amount of alumina increases consistently with the maturation temperature of the glassy material. Likewise, glass is ZnO free and the porcelain single firing frit (1190 $^{\circ}\text{C}$) show a low amount of ZnO (6 wt%) compared with double firing 1050 $^{\circ}\text{C}$ (9 wt%) or single firing 1080 $^{\circ}\text{C}$ (7.5 wt%).

Figure 2.a shows the UV-Vis diffuse reflectance spectra of glazes with detection of an intense charge-transfer absorption associated to a classic wide bandgap semiconductor behaviour, with inflection point of 407 nm (not shown) for glass, 335 nm for porcelain single firing 1190 $^{\circ}\text{C}$, 325 nm for single firing 1080 $^{\circ}\text{C}$

and 315 nm for double firing 1050 $^{\circ}\text{C}$ glaze, and associated bandgap of 3.05, 3.70, 3.82 and 3.93 eV respectively. As above-mentioned, the high UV absorption of glazes is interesting for block UV radiation and protect possible organic binders.

Sb_2O_3 exist in two crystalline polymorphs cubic (senarmonite or $\alpha\text{-Sb}_2\text{O}_3$) and orthorhombic (valentinite or $\beta\text{-Sb}_2\text{O}_3$) both semiconductor (direct p type with inflection point in UV around 340 nm for α and 390 for β). It is widely used as a filler for paints and polymers (as a white pigment, UV filter, adhesion agent, light scatterer, and fire retardant) and in the production of semiconductors, sorbents, catalysts, conducting polymers, and other materials [19]. Composite oxides including antimony show catalytic activity and selectivity in the reactions of organic synthesis. Their sorption properties that allow producing ion-exchange materials, molecular sieves, and ion-selective sorbents are also of interest [16].

Figure 2-b shows the UV-Vis-NIR reflectance spectra of $\beta\text{-Sb}_2\text{O}_3$ oxide (used as SSA modifier of the copper-chromium oxide), CuO and carbon black (COAL) powders. The white $\beta\text{-Sb}_2\text{O}_3$ oxide shows high reflectance values on visible range (R_{Vis}), on NIR (R_{NIR}) and total reflectance (R): $R_{\text{Vis}}/R_{\text{NIR}}/R$ (%) =

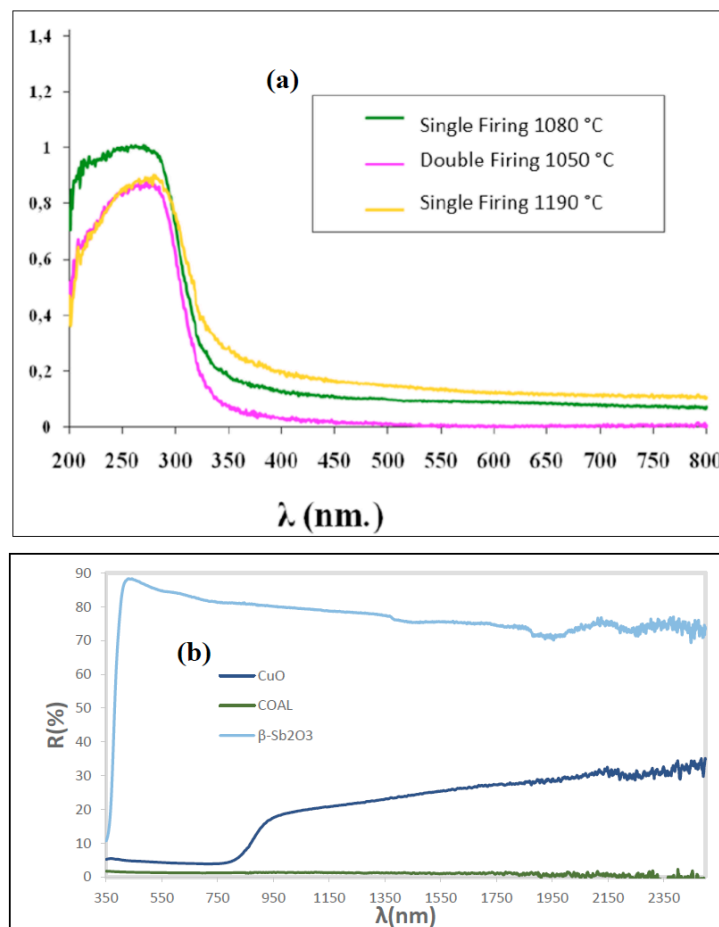


Figure 2: UV-Vis diffuse reflectance spectra: (a) employed ceramic glazes, (b) $\beta\text{-Sb}_2\text{O}_3$ oxide, CuO and carbon black (COAL) powders used as references.

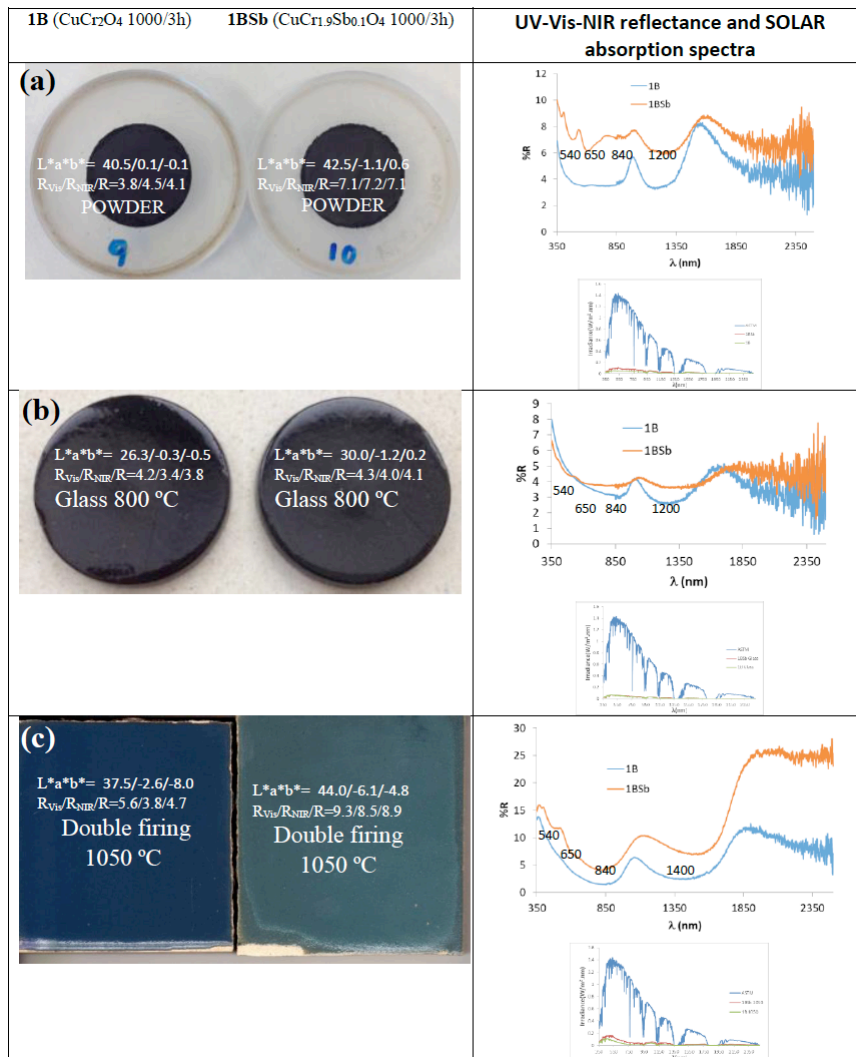
Table 2: Colour and Reflectance Characteristics of Samples

Sample	$L^*a^*b^*$	$R_{\text{vis}}/R_{\text{NIR}}/R$ (%)	ΔE^*	C^*	h	α	ϵ_{100}	$E_g(\text{eV})$
1B	40.5/0.1/-0.1	3.8/4.5/4.1	20.3	0.14	135.0	0.96	0.78	1.30
1BSb	42.5/-1.1/0.6	7.1/7.2/7.1	22.3	1.25	151.4	0.93	0.76	1.28
1B Glass	26.3/-0.3/-0.5	4.2/3.4/3.8	6.1	0.58	239.0	0.97	0.80	1.31
1BSb Glass	30.0/-1.2/0.2	4.3/4.0/4.1	9.9	1.21	170.5	0.96	0.79	1.31
1B 1050	37.5/-2.6/-8.0	5.6/3.8/4.7	19.3	8.4	252.0	0.96	0.75	0.80
1BSb 1050	44.0/-6.1/-4.8	9.3/8.5/8.9	25.1	7.8	218.2	0.92	0.62	0.78
1B 1080	45.8/-3.6/-5.7	10.8/8.6/9.7	25.8	3.26	152.7	0.91	0.66	0.88
1BSb 1080	49.3/-6.2/-1.9	15.2/17.6/16.4	29.8	6.50	197.0	0.82	0.42	0.88
1B 1190	32.1/-1.3/0.8	5.9/14/9.9	12.0	1.52	148.4	0.86	0.45	0.90
1BSb 1190	38.0/-3.2/3.1	8.8/22.4/15.4	18.4	4.50	135.9	0.78	0.30	0.92
CuO	25.8/0.3/-2.4	5.1/21.2/12.2	6.3	2.41	83.1	0.89	0.69	1.40
C	20.2/0.1/0.1	3/3/3		0.14	45	0.99	0.96	1.40

83.3/80.1/81.2. Figure 2 shows an intense charge-transfer absorption with inflection point of 390 nm (associated bandgap of 3.2 eV). CuO and carbon black are used as SSA and black colour references respectively, its optical parameters are shown in Table 2.

3.2. Characterization of Powders

Figure 3a and Table 2 show the characteristics of black powders 1B and 1BSb: tetragonal CuCr_2O_3 (sample 1B) shows a better black shade than antimony modified sample $\text{Cu}(\text{Cr}_{1.9}\text{Sb}_{0.1}\text{O}_4)$ (1BSb) (lower a^* and



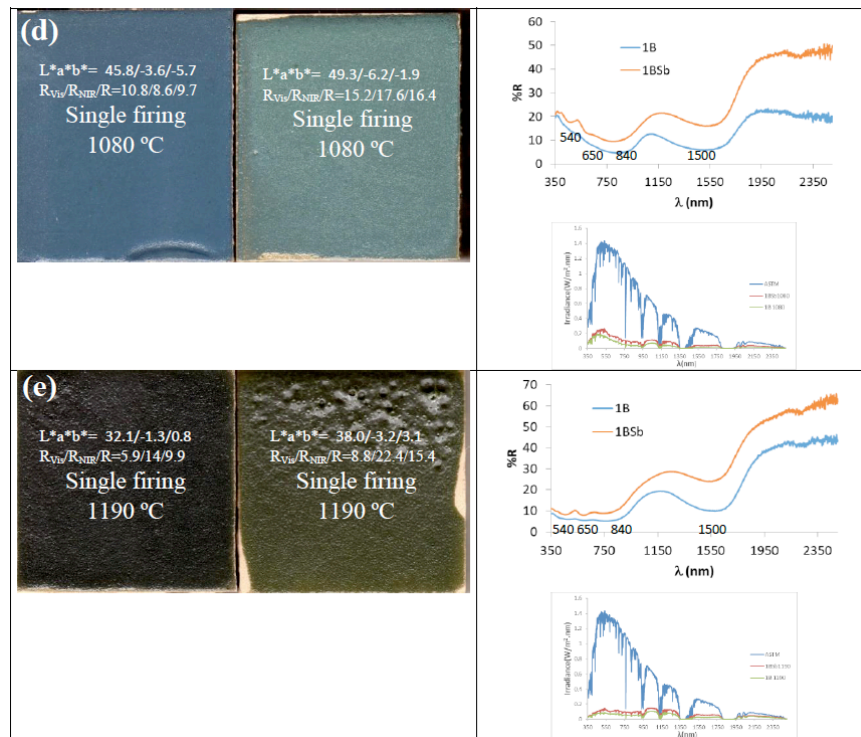


Figure 3: t-CuCr₂O₄ powders and glazed sample image with its colour and reflectance characteristics (summarized in Table 1 using as reference a commercial carbon black ($L^*a^*b^*=20.2/0.1/0.1$, $R_{vis}/R_{NIR}/R = 3/3/3$, $C^*=0.14$, $h=45$)).

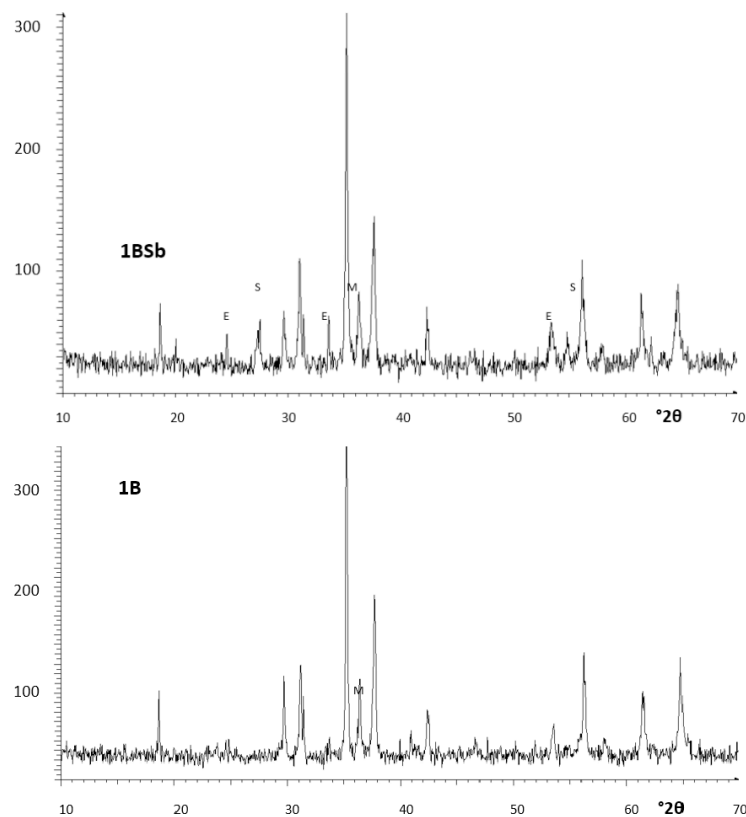


Figure 4: XRD of samples: CRYSTALLINE PHASES: E (Cr₂O₃), S (SbO₂), M (CuFeO₂).

b*) although its brightness L^* is very similar (40.5 and 42.5 respectively) higher than the corresponding to carbon black ($L^*=20$) used as powder reference. In effect, the colour deviation ΔE^* from the carbon black

reference is 20.3 and 22.3 for CuCr₂O₃ (sample 1B) and Cu(Cr_{1.9}Sb_{0.1}O₄) (sample 1BSb) respectively.

Figure 4 shows the XRD diffractograms of both samples: in the case of 1B the tetragonal CuCr₂O₃

Table 3: Elemental Cell Parameters of Tetragonal CuCr₂O₄ of 1B and 1BSb Samples

Sample	a=b (Å)	c (Å)	V (Å ³)
1B	6.026(4)	7.800(9)	283(5)
1BSb	6.031(5)	7.967(8)	289(2)

(JCPDS 034-0424) is the only crystalline phase detected on the powder with a weak peak at $36.5^\circ 2\theta$ of delafossite CuCrO₂. In the composite, very low diffraction peaks associated to eskolaite Cr₂O₃ (JCPDS 051-0959), and the variable valence compound cervantite, Sb₂O₄ (Sb³⁺Sb⁵⁺O₄) (JCPDS 037-0854) [20], are also detected, forming a homogeneous composite with tetragonal CuCr₂O₄. The XRD detection of the both stoichiometric components of the composition would indicate some entrance of antimony in solid solution into tetragonal CuCr₂O₄. The direct measurement of tetragonal lattice parameters, using equation 3 from the XRD peak positions of tetragonal CuCr₂O₄ in 1B and 1BSb powders, are shown in Table 3: the unit cell of tetragonal CuCr₂O₄ increases in the antimony modified sample 1BSb, in accordance with some entrance of the larger Sb³⁺ (0.9 Å Shannon-Prewit ionic radius [21] in octahedral coordination) replacing the smaller Cr³⁺ (0.755 Å Shannon-Prewit ionic radius in octahedral coordination) in the tetragonal lattice.

Figure 3.a (right) shows the UV-Vis-NIR reflectance spectra of powders. Absorbance bands (minima in the figure) at 540, 650, 800 and 1200 nm can be observed for 1B sample. The Cu²⁺ of CuO₄ tetrahedra compressed toward a square planar configuration showing square-plane coordination is observed as in the Mn-Melilite and the Egyptian Blue pigments [22, 23]: it shows weak d-d transitions of copper with bands at 800 nm associated with (²B_{1g} → ²B_{2g}), at 650 nm with (²B_{1g} → ²E_g) and at 540 nm with (²B_{1g} → ²A_{1g}). On the other hand, Cr³⁺ (d³) absorptions in octahedral environments overlapps its bands at 450 nm (⁴A_{2g}(4F) → ⁴T_{1g}(4F)), the usually detected at 680 nm (⁴A_{2g}(4F) → ⁴T_{2g}(4F)) and the band at 1200 nm (⁴A_{2g}(4F) → ²E_g(2G)). Therefore the overlapping of absorption bands of Cr³⁺ (d³) in octahedral coordination and Cu²⁺ ions in square-plane coordination can explain the reflectance spectra. However, the intensity of these d-d transitions does not justify the anomalously high optical density detected. Therefore, as in the case Mn-Melilite and the Egyptian Blue pigments, an spin-exchange interactions of Cr³⁺ with adjacent Cu²⁺ by a paired spin exchange transition (PET), should be considered [14]. Figure 5 shows the evolution of UV-Vis-NIR reflectance spectra of samples with the different glazes (soda lime glass 800 °C, double firing glaze 1050 °C, single firing

glaze 1080 °C and single firing porcelain glaze 1190 °C) compared with the parent powder.

The entrance of Sb³⁺ in solid solution into tetragonal CuCr₂O₄, above described, can be associated to the shift to higher wavelengths of these absorption bands (and the corresponding maximums of reflectance) in the 1BSb sample. The spectrum shows better resolution, although the whole reflectance of the sample increases causing a lower black response of the material. The reflectance solar spectra of powders compared with the solar light (Figure 3.a (right)), shows the high solar absorption of these black powders.

Figure 6 shows the SEM micrographs and the EDS compositional mapping of the powders. Both powders show fine particles around 0.5-2 μm and 1-3 μm of particle size for 1B and 1BSb samples respectively. EDS mapping shows a homogeneous distribution of Cu and Cr ions in all particles of both powders; however, Sb shows also some individual particles in 1BSb powders, in agreement with the XRD results.

Figure 7.a summarises the Tauc plot of samples, both powders show a direct semiconductor behaviour with bandgap of 1.30 and 1.28 eV for 1B and 1BSb respectively in agreement with literature [12]. As above discussed, for SSA surfaces the spectral transition between the region of high absorbance and low emittance (cut-off wavelength) should be as sharper possible and, in practice, for energy applications, should be around 2000 nm, which is the limit of the solar spectrum [6]. The absorbance of Vis-NIR Solar Radiation (α) evaluated by equation 1 are 96% and 93% for 1B and 1BSb powders respectively. The cut-off of the t-CuCr₂O₄ powders is out of the NIR range (>2500 nm) and shows relative high emittance (ε) (0.78 and 0.76 for 1B and 1BSb respectively), showing selective solar absorption.

3.3. Tetragonal CuCr₂O₄ in Soda-Lime Glass (0.5wt%)

Figure 3.b and Table 2 show the characteristics of 0.5wt% glazed powders in soda-lime glass fired at 800 °C. As in powder samples, sample 1B shows a better black shade than antimony modified sample 1BSb: lower a* but slightly higher b*, with brightness L*

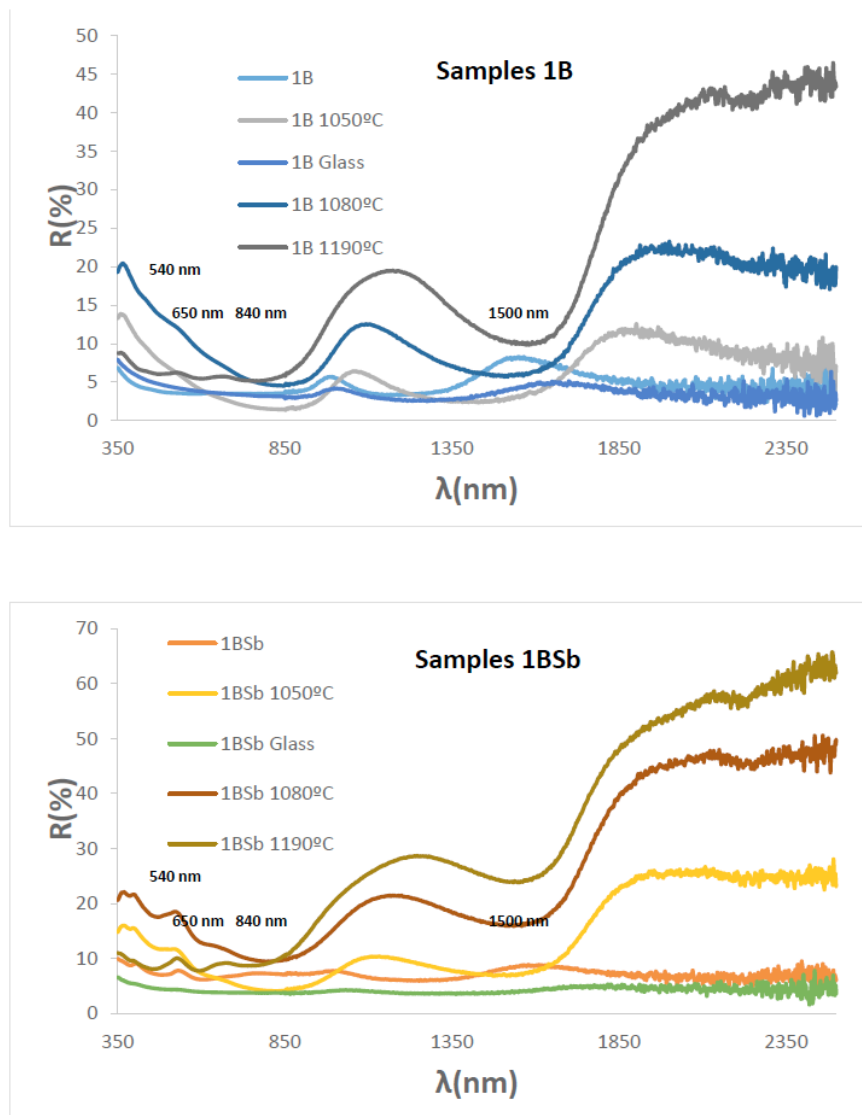


Figure 5: Evolution of UV-Vis-NIR reflectance spectra of samples with different glazes.

similar (26.3 and 30.0 respectively) closer than powders to carbon black ($L^*=20$) with $\Delta E^*=6.1$ and 9.9 respectively (Table 2).

Figure 3.b (right) shows the UV-Vis-NIR reflectance spectra of glass samples. It can be detected the same absorbance bands than for powders at 540, 650, 800 and 1200 showing the stability of the pigment in the glass. The reflectance in Vis, NIR and total range R of both glass samples is very similar (around 4%) and it can be observed a slight shift of bands to higher wavelengths for antimony modified sample as in the case of powders. The reflectance solar spectra Figure 3.a (right), shows the high solar absorption of the black glasses.

Figure 7.b shows the Tauc plot of samples with a direct semiconductor behaviour and bandgap of 1.31 eV for both samples in agreement with literature [12]. The absorbance of glass samples (α) evaluated by equation 1 is 97% and 96% for 1B and 1BSb coloured

glass respectively (Table 2). As in the case of powders, the cut-off of absorption of the glass samples is out of the NIR range (>2500 nm) and show relative high emittance (ϵ) (0.80 and 0.79 for 1B and 1BSb respectively) showing selective solar absorption, similar to powders.

3.2. Tetragonal CuCr_2O_3 in Double Firing Glaze 1050 °C (5wt%)

Figure 3.c and Table 2 show the characteristics of 5wt% glazed powders in the double firing glaze fired at 1050 °C. Tetragonal CuCr_2O_3 1B sample produces blueish glazes ($b^* = -8$) and the antimony modified 1bSB greenish ($a^* = -6.5$) indicating a partial exsolution of copper from the pigments. In effect, Cu^{2+} solved in glazes can produce green colour associated to octahedral Cu^{2+} in the glassy matrix or blue colour associated to Cu^{2+} square planar coordinated of oxygens of the glass [24]. Therefore, in the case of sample 1B, the Cu^{2+} exsolved in the glaze is

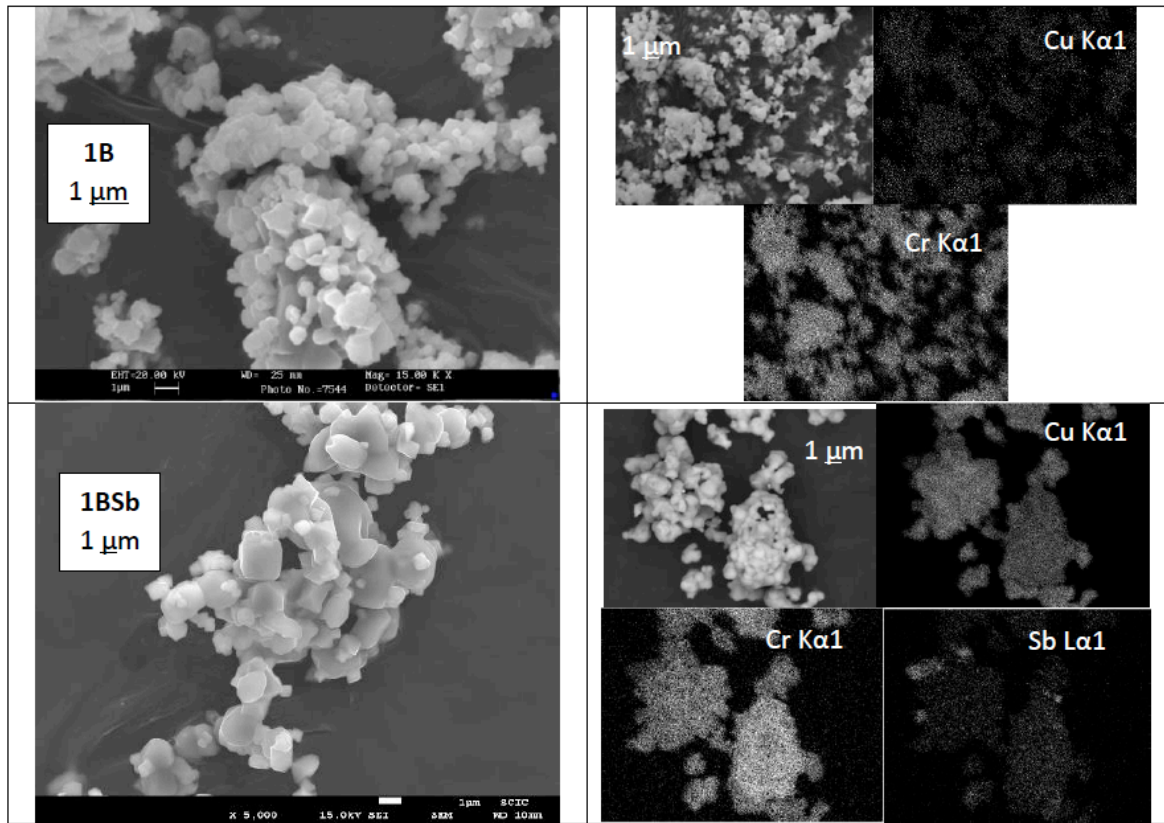
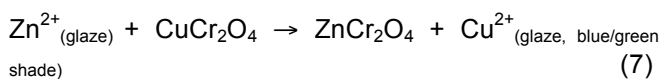


Figure 6: SEM-EDS of powders.

predominantly square planar coordinated, and octahedral in the case of antimony modified sample.

The instability of the pigment, which is partially dissolved by the molten glaze, is well known in the literature [25, 26]; the glaze reacts with tetragonal CuCr_2O_4 to produce highly stable spinels, reacting with the Zn^{2+} of the glaze and producing the high stable zincochromite:



The absence of Al^{3+} and Zn^{2+} in the case of soda-lime glass, avoids the above reactions, preserving the stability of the pigment in the molten glass. The presence of the acidic antimony modifies the glassy lattice and explain the loss of the blue shade associated to square planar Cu^{2+} promoting the octahedral Cu^{2+} coordination in the glassy matrix: in effect, it is well known in literature that the alkali metal enriched glaze shows cyan or lake blue features, and it becomes green when adding more acidic compositions (e.g., phosphorous or antimony additions) [27].

Figure 3.c (right) shows the UV-Vis-NIR reflectance spectra of 5wt% glazed samples with the double firing glaze at 1050 °C. It can be detected the same absorbance bands than for powders at 540, 650, 800 but the band at 1200 nm shifts to 1400 nm and appears

more resolved. This behaviour is in accordance with the observed instability of the colour in the glaze producing blue and green shades. The reflectance in Vis, NIR and total range R of green 1BSb sample is higher than in blue 1B sample (R=8.9 and 4.7 respectively). However, the reflectance of 1B is very close to powder and glass samples. It can be observed the shift of bands to higher wavelengths for antimony modified sample as in the previous cases. The solar spectra Figure 3.a (right) shows the high solar absorption of the blue 1B sample and highlights some reflectance of the green antimony modified glaze.

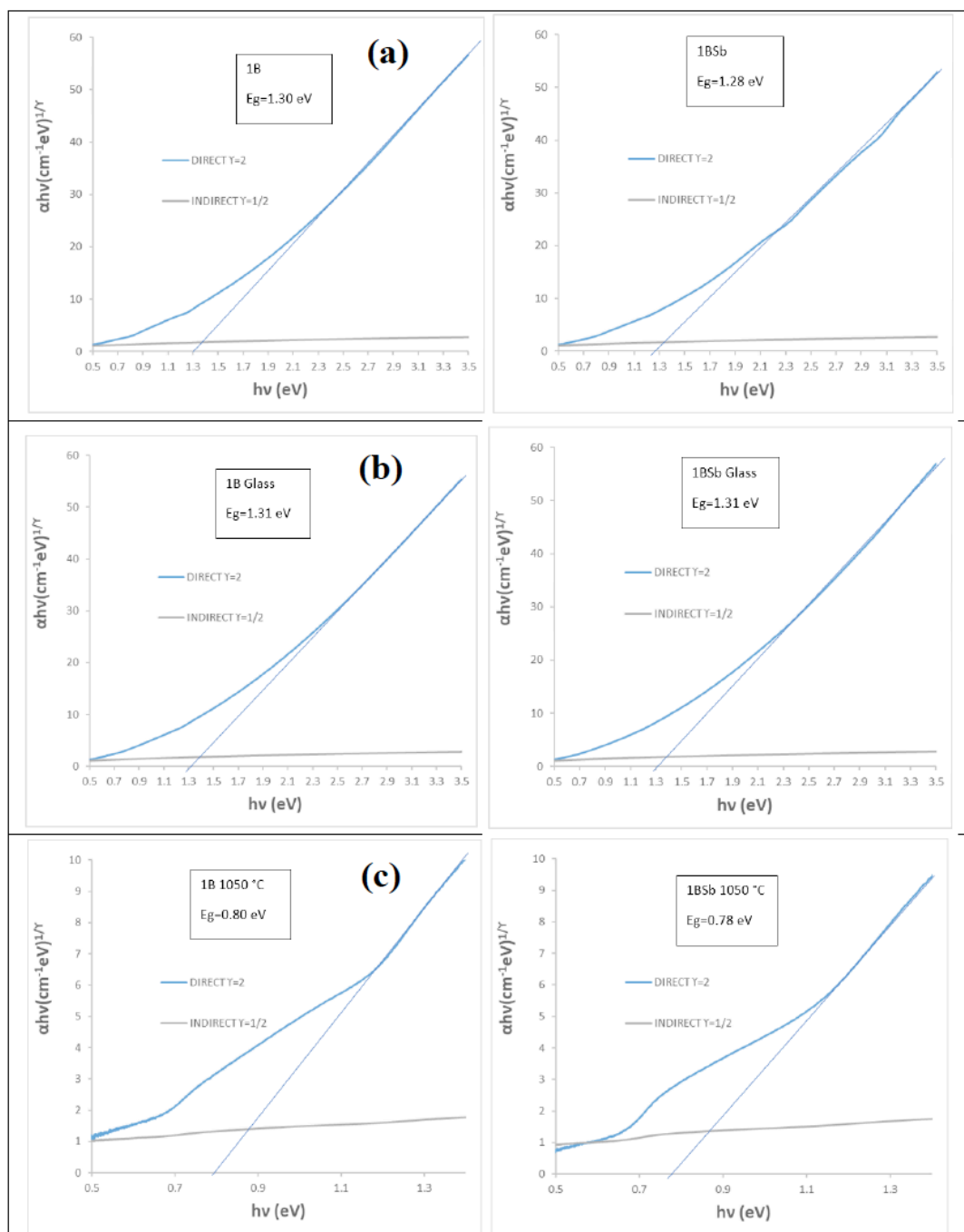
Figure 7.c summarises the Tauc plot of samples. Both glazed samples show a direct semiconductor behaviour with bandgap of 0.80 and 0.78 eV for 1B and 1BSb lower than values measured for powders and glass samples associated to the increase of reflectance from 1550 nm with inflection point around 1750 nm in these glazed samples. In effect, the absorbance of this samples (α) is 96% and 92% for 1B and 1BSb samples respectively (Table 2). The cut-off of absorption of the glazed samples is practically out of the NIR range (>2500 nm) for blue 1B sample which shows a weak cut-off with inflection point at 1725 nm with only R=10%. However, the green sample 1BSb already shows a clear cut-off of absorbance with inflection point at 1780 nm to 25% of reflectance. Therefore, the 1B glazed sample shows relative high emittance which decreases

in the green 1BSb glazed sample showing a better selective solar absorption.

3.3. Tetragonal CuCr_2O_3 in Single Firing Glaze 1080 °C (5wt%)

Figure 3.d and Table 2 show the characteristics of 5wt% glazed powders in the single firing glaze fired at 1080 °C (monoporosa). As in the double firing glaze, 1B sample produces blueish glazes ($b^* = -5.7$) and the antimony modified 1BSb greenish ($a^* = -6.2$), associated to the above discussed partial exsolution of copper from the pigments: in the case of sample 1B, the Cu^{2+} exsolved in the glaze is predominantly square planar coordinated, and octahedral in the case of

antimony modified sample. The intensity of the colour is lower in this glaze than in the corresponding samples with the double firing glaze ($L^* = 45.8$ and 49.3 versus 37.5 and 44.0 for the blue and green samples in respectively glazes) (Table 2). However, the blue value of 1B sample decreases respect the sample with the double firing 1050 °C (-5.8 versus -8) and also for the 1BSb respect its homologous sample in the double firing 1050 °C sample ($b^* = -1.9$ versus -4.8), however, the green shade in the 1BSb is similar in the both glazes. The decrease in colour intensity agrees with the higher solving action of the single firing glaze. however, the lower presence of Zn^{2+} in the glaze, in accordance with solving equation 7, moderates the



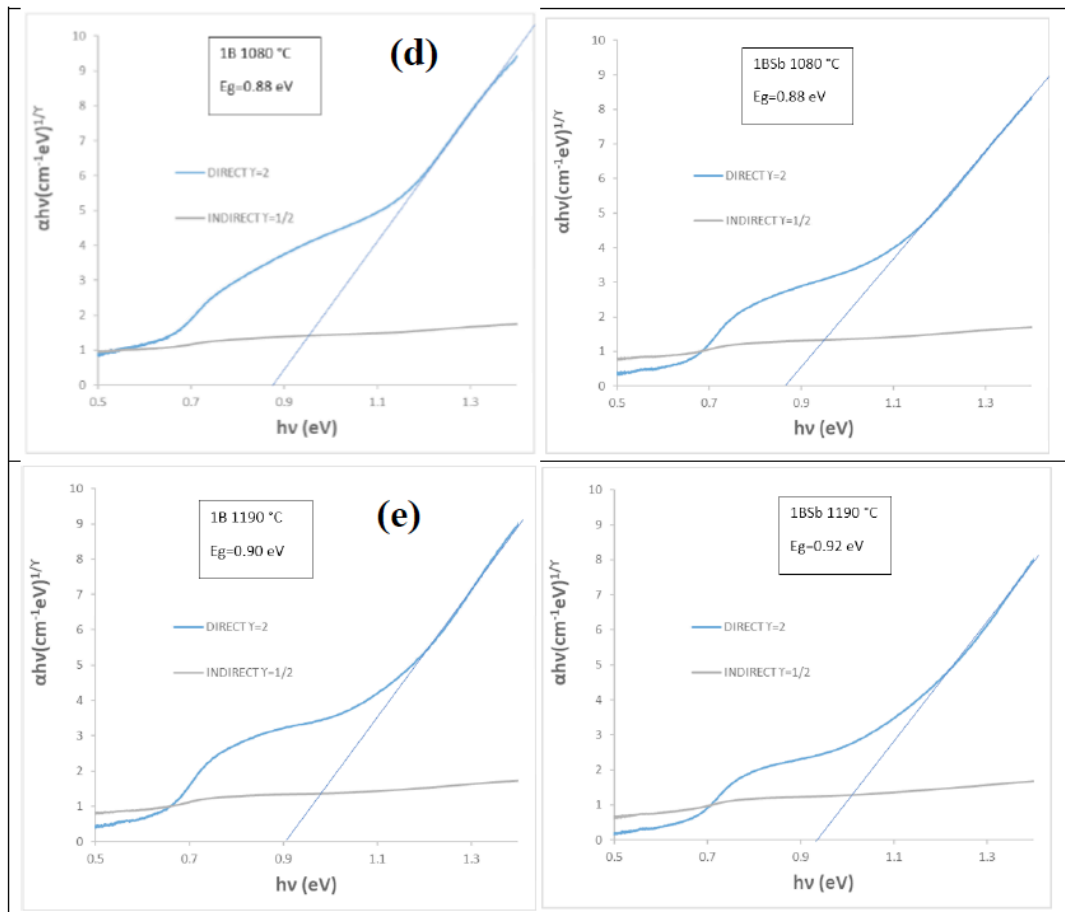


Figure 7: Tauc plot of indicated samples.

change in colour shade, and the chroma C^* is lower in both samples than in the double firing 1050 °C glaze.

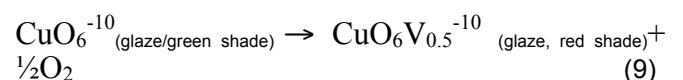
Figure 3.d (right) shows the UV-Vis-NIR reflectance spectra of 5wt% glazed samples with the single firing glaze at 1080 °C. It can be detected the same absorbance bands than for powders at 540, 650, 800 but the band at 1200 nm shifts to 1500 nm and appears more resolved than in the double firing glaze in accordance with the observed instability of the colour in the glaze producing blue and green shades. The reflectance in Vis, NIR and total range R of green 1BSb sample are higher than in blue 1B sample ($R=17.6$ and 8.6 respectively) and double the values in the previous double-firing glaze. The shift of bands to higher wavelengths for antimony modified sample, as in the previous cases, is detected, and the reflectance solar spectra Figure 3.d (right), now shows some reflectance in the two samples.

Figure 7.d summarises the Tauc plot of samples, both glazed samples show a direct semiconductor behaviour with bandgap of 0.88 eV for both 1B and 1BSb samples, similar to previous samples with glaze of 1050 °C, associated to the increase of reflectance from 1600 nm. As in the previous glazed samples, the

value of absorbance for this samples (α) is 91% and 82% for 1B and 1BSb samples respectively (Table 2). The cut-off of absorption of the blue 1B sample shows an inflection point at 1700 nm with $R=20\%$, and for the green sample 1BSb at 1720 nm with 40% of reflectance. Therefore, the emittance decreases in both glazes showing a better selective solar absorption.

3.4. Tetragonal CuCr_2O_3 in Porcelain Single Firing Glaze 1190 °C (5wt%)

Figure 3.e and Table 2 show the characteristics of 5wt% glazed powders in the single firing glaze fired at 1190 °C (porcelain glaze). In this case, 1B sample produces black glazes ($L^*a^*b^*=32.1/-1.3/0.8$ with chroma C^* of 1.52) and the antimony modified 1BSb greenish ($L^*a^*b^*=38.0/-3.2/3.1$) associated to exsolved Cu^{2+} square planar coordinated. Some pin-hole defects are observed in 1BSb sample associated to a partial reduction to Cu^+ (it is well known the evolving oxygen that causes the observed pin-hole [28], considering the local ionic equilibria in the glassy network ($V=\text{oxygen ion vacancy}$):



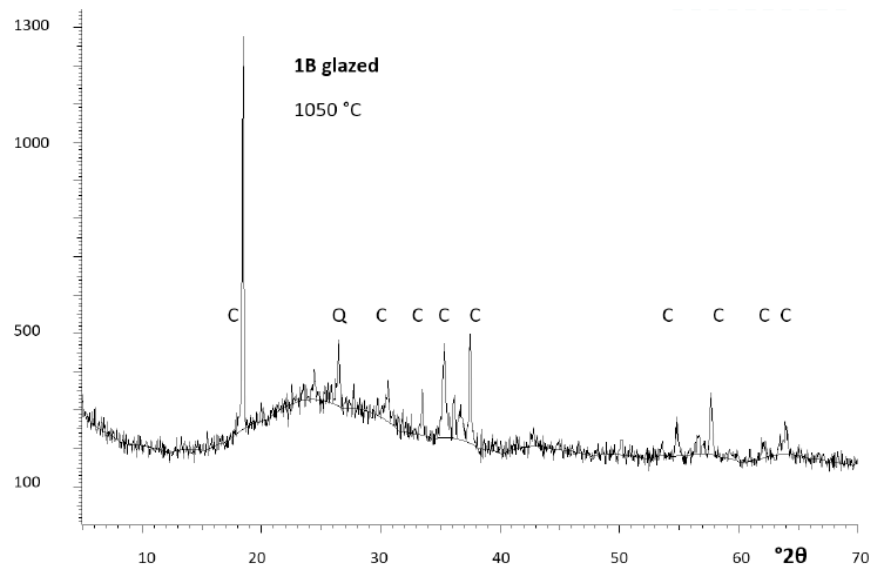


Figure 8: Grazing X-ray diffraction diffractogram of 5wt% glazed sample in the double glaze at 1050 °C: CRYSTALLINE PHASES: Q (quartz), C (t-CuFe₂O₄).

The intensity of the colour is higher in this glaze than in the previous glazes (low L^* , Table 2) associated to the higher stability of the pigment in this porcelain glaze producing black shades, probably associated to the low amount of Zn in the glaze, avoiding the interaction described by eq. 7.

Figure 3.e (right) shows the UV-Vis-NIR reflectance spectra of 5wt% glazed samples with the single firing glaze at 1190 °C. It can be detected the same absorbance bands than for powders at 540, 650, 800 nm but the band at 1200 nm shifts to 1500 nm well resolved. As in the previous glazes, the reflectance in Vis, NIR and total range R of 1BSb sample are higher than in 1B sample ($R=15.4$ and 9.9 respectively) similar to those measured in the single fire frit 1080 ° and double the values in the previous double-firing glaze. The shift of bands to higher wavelengths for antimony modified sample, as in the previous cases, is detected, and the reflectance solar spectra Figure 3.e (right), show very low reflectance associated to black appearance of the glaze.

Figure 7.e shows the Tauc plot of samples which show a direct semiconductor behaviour with bandgap of 0.90 and 0.92 eV for 1B and 1BSb samples respectively, slightly higher than in the previous glazed samples, associated with the increase of reflectance from 1600 nm. As in the previous glazed samples, the value of absorbance for these samples (α) are 86% and 76% for 1B and 1BSb samples respectively (Table 2). The cut-off of absorption of the blue 1B sample shows a inflection point at 1720 nm with $R=40\%$, and for the green sample 1BSb at 1740 nm with 50% of reflectance. Therefore, the emittance decreases in both

glazes, showing the best selective solar absorption behaviour for to be applied as SAS coating for an integral ceramic solar collector.

Finally, to check the stability of the tetragonal cuprochromite crystalline phase in the glazes, the 5wt% glazed sample in the double glaze at 1050 °C was studied by grazing or low angle of incidence X-ray diffraction, carried out on a Siemens D5000 diffractometer using similar conditions that for conventional diffractometry. Figure 8 shows the diffractogram where the silica halo centered at 25 °2 θ together with peaks associated with the crystallization of quartz from the devitrification of the glass [29] and the peaks associated with t-CuCr₂O₄ that remained stable within the glaze [30].

4. CONCLUSIONS

Coloured glazes of t-CuCr₂O₄ black pigment with industrial glazes with increasing temperature (milled soda-lime glass (800 °C), double firing frit (1050 °C), single firing frit (1080°C) and single firing porcelain frit (1190 °C) have been characterised as selective solar absorber (SSA) for integral ceramic solar collectors. Tetragonal CuCr₂O₄ and the solid solution Sb-CuCr₂O₄ and valentinite (β -Sb₂O₃) composite with formal stoichiometry Cu(Cr_{1.9}Sb_{0.1}O₄) have been prepared by solid state reaction method from oxides. The characteristics of the black powders ($L^*a^*b^*$ and diffuse reflectance spectra with a deviation from the carbon black $\Delta E^*=20.3$ and 22.3 respectively) are improved in 0.5 wt% addition of pigments in glass ($\Delta E^*=6.1$ and 9.9 respectively) and in 5 wt% glazed in porcelain glaze 1190 °C ($\Delta E^*=12.0$ and 18.4 respectively with a sharp

cut of reflectance at 1720 and 1740 nm respectively) which can be considered as low-cost selective solar absorber (SSA) for integral solar absorber collectors. 5 wt% glazed samples in double firing glaze 1050 °C or in single firing glaze 1080 °C blueish or greenish associated to solving effect of these glazes over copper. However, both also show interesting characteristics as low-cost selective solar absorbers for integral solar absorber collectors.

CONFLICTS OF INTEREST

The authors declare that they have no conflict of interest related to this work.

ACKNOWLEDGEMENT

The authors acknowledge Jaume I University (UJI) and Valencian Community Government (GV) its financial support (UJI-B2021-73 and CIAICO/2022/155 projects, respectively), and the technical support of the Servei Central d'Instrumentació Científica (SCIC) (UJI).

REFERENCES

- [1] Yang H., Wang Q., Huang Y., Feng J., Ao X., Hu M., Pei G., Spectral optimization of solar selective absorbing coating for parabolic trough receiver, *Energy*, 2019; 183: 639-650. <https://doi.org/10.1016/j.energy.2019.06.090>
- [2] Tena M.A., Mestre A., García A., Sorlí S., Monrós G., Synthesis of Gray Ceramic Pigments with Rutile Structure from Alkoxides, *Journal of Sol-Gel Science and Technology*, 2003; 26: 813-816. <https://doi.org/10.1023/A:1020743531408>
- [3] CPMA Classification and chemical description of the complex inorganic color pigments, fourth ed. Alexandria, Dry Color Manufacturers Association, 2010.
- [4] Yang Y., Cao S., Xu J., Cai B., All-ceramic solar collectors, *Ceramics International*, 2013; 39: 6009-6012. <https://doi.org/10.1016/j.ceramint.2013.01.011>
- [5] Shanker V., Holloway P.H., Electrodeposition of black chrome selective solar absorber coatings with improved thermal stability, *Thin Solid Films* 1985; 127: 181-189. [https://doi.org/10.1016/0040-6090\(85\)90189-0](https://doi.org/10.1016/0040-6090(85)90189-0)
- [6] Roberts D.E., Forbes A., An analytical expression for the instantaneous efficiency of a flat plate solar water heater and the influence of absorber plate absorptance and emittance, *Solar Energy*, 2012; 86: 1416-1427. <https://doi.org/10.1016/j.solener.2012.01.032>
- [7] Kennedy C.E., Review of Mid- to High-Temperature Solar Selective Absorber Materials, 2002. <https://doi.org/10.2172/15000706>
- [8] Kuhn, T. S. (1978). *Black-Body Theory and the Quantum Discontinuity*. Oxford University Press. ISBN 0-19-502383-8
- [9] Suchomei M.R., Shoemaker D.P., Ribaud L., Kemei M.C., Seshadri R. Spin-induced symmetry breaking in orbitally ordered NiCr_2O_4 and CuCr_2O_4 , *Physical Review*, 2012; B 86: 054406. <https://doi.org/10.1103/PhysRevB.86.054406>
- [10] Acharyya S.S., Ghosh S., Tiwari R., Sarkar B., Singha R.K., Pendem C., Sasaki T., Bal R., Preparation of the CuCr_2O_4 Spinel Nanoparticles Catalyst for Selective Oxidation of Toluene to Benzaldehyde, *Green Chem.*, 2014; 16: 2500-2508. <https://doi.org/10.1039/C3GC42369G>
- [11] Ma P., Geng Q., Gao X., Yang S., Liu G., CuCr_2O_4 Spinel Ceramic Pigments Synthesized by Sol-Gel Self-Combustion Method for Solar Absorber Coatings, *Journal of Materials Engineering and Performance*, 2016; 25.7: 2814-2823. <https://doi.org/10.1007/s11665-016-2143-z>
- [12] Paul B., Bhuyan B., Purkayastha D.D., Dhar S. S., Behera S., Facile synthesis of spinel CuCr_2O_4 nanoparticles and studies of their photocatalytic activity in degradation of some selected organic dyes, *Journal of Alloys and Compounds* 2015; 648: 629-635. <https://doi.org/10.1016/j.jallcom.2015.07.012>
- [13] Monrós G. (2014), Pigment, Ceramic in *Encyclopedia of Color Science and Technology*, Ronnier Luo ed., Springer, New York. <http://www.springerreference.com/docs/html/chapterdbid/348055.html>.
- [14] Monrós G. (2021), Scheelite and Zircon: Brightness, Color and NIR Reflectance in Ceramics, Nova Scienc Publishers, New York, ISBN: 978-1-53619-332-9
- [15] ACGIH (American Conference of Governmental Industrial Hygienists), <https://www.acgih.org/science/tlv-bei-guidelines/tlv-chemical-substances-introduction/>
- [16] Zemnukhova L.A., Panasenko A.E., A novel composite material based on antimony(III) oxide and amorphous silica, *Journal of Solid State Chemistry* 2013; 201: 9-12. <https://doi.org/10.1016/j.jssc.2013.02.005>
- [17] CIE Comission International de l'Eclairage, Recommendations on Uniform Color Spaces, Colour Difference Equations, Psychometrics Colour Terms. Supplement n°2 of CIE Pub. N°15 (E1-1.31) 1971, Bureau Central de la CIE, Paris (1978).
- [18] Munsell, A.H. (1915), *Atlas of the Munsell color system*, Malden, Mass., Wadsworth, Howland & Co., inc. Printers. <https://doi.org/10.5479/sil.129262.39088002718880>
- [19] Panasenkoa A.E., Zemnukhovaa L.A., Barinov N.N., Morphology and Optical Properties of Sb_2O_3 . *Inorganic Materials*, 2010; 46,4: 389-392. <https://doi.org/10.1134/S0020168510040126>
- [20] Amador J., Gutierrez Puebla E., Monge, M.A., Rasines I., Ruiz Valero C., Diantimony Tetraoxides Revisited. *Inorganic Chemistry*, 1988; 27,8: 1367-1370. <https://doi.org/10.1021/ic000281a011>
- [21] Shannon, R. D., Revised effective ionic radii and systematic studies of interatomic distances in halides and chalcogenides, *Acta Cryst.* 1976; A32: 751. <https://doi.org/10.1107/S0567739476001551>
- [22] Monrós G., Cerro S., Badenes J.A., Llusar M.I., Black Cool Pigments for Urban Heat Island (UHI) Control: from Cr-Hematite to Mn-Melilite, *Journal of Solar Energy Research Updates*, 2021; 8: 27-44. <https://doi.org/10.31875/2410-2199.2021.08.4>
- [23] Kendrick E., Kirk C.J., Dann S.E., Structure and colour properties in the Egyptian Blue Family, $\text{M}_{1-x}\text{M}'_x\text{CuSi}_4\text{O}_{10}$, as a function of M, M' where M, M'=Ca, Sr and Ba. *Dyes Pigm* 2007; 73: 13-18. <https://doi.org/10.1016/j.dyepig.2005.10.006>
- [24] Peng I., Hills-Kimball K., Miñana Lovelace I., Wang J., Rios M., Chen O., Wang L., Exploring the Colors of Copper-Containing Pigments, Copper (II) Oxide and Malachite, and Their Origins in Ceramic Glazes, *Colorants* 2022; 1(4): 376-387. <https://doi.org/10.3390/colorants1040023>
- [25] Verger, L., Olivier D., Rouse, G., Cotte, M., Cormier L, The Stability of Gahnite Doped with Chromium Pigments in Glazes from the French Manufacture of Sèvres. *Journal of the American Ceramic Society*, 2016; 100(1): 86-95. <https://doi.org/10.1111/jace.14452>
- [26] Verger, L.; Olivier D.; Rouse, G.; Cormier L, G., Reactivity of chromium-based pigments in a porcelain glaze, *C. R. Physique* 19 (2018) 589-598. <https://doi.org/10.1016/j.cryh.2018.09.008>
- [27] Zhang B, Zhu J., Shi P., Wang F., Wang J., Ren Z., Achieving tunable sky-blue copper glaze and coloring mechanism by the introduction of phosphorus. *Journal of the*

- European Ceramic Society 2019; 39,5: 1925-1931.
<https://doi.org/10.1016/j.jeurceramsoc.2019.01.025>
- [28] Kaufmann J., Rüssel C., Thermodynamics of the Cu⁺/Cu²⁺-redox equilibrium in aluminosilicate melts, *J. Non-Cryst. Solids* 2010; 356(33-34): 1615-1619.
<https://doi.org/10.1016/j.jnoncrysol.2010.06.032>
- [29] Ali A., Disher I., The devitrification kinetics of transparent silica glass prepared by gel-casting method, *Revistamateria*, 2019; 24(1): 1-9.
<https://doi.org/10.1590/s1517-707620190001.0654>
- [30] Monrós G., LLusar M.I., Badenes J.A., Sol-Gel ceramic glazes with photocatalytic activity, *Journal of Sol-Gel Science and Technology*, 2022: 102(3) 535-549. (2022) 102: 535-549.
<https://doi.org/10.1007/s10971-022-05787-z>

Received on 04-11-2024

Accepted on 21-12-2024

Published on 30-12-2024

<https://doi.org/10.31875/2410-2199.2024.11.09>

© 2024 Monrós *et al.*

This is an open-access article licensed under the terms of the Creative Commons Attribution License (<http://creativecommons.org/licenses/by/4.0/>), which permits unrestricted use, distribution, and reproduction in any medium, provided the work is properly cited.